JOURNAL OF SOLID STATE CHEMISTRY 105, 458–468 (1993)

Electrochemical Preparation and Structural Characterization of $La_2NiO_{4+\delta}$ Phases ($0 \leq \delta \leq 0.25$)

A. DEMOURGUES, A. WATTIAUX, J. C. GRENIER, M. POUCHARD, J. L. SOUBEYROUX, J. M. DANCE, AND P. HAGENMULLER

Laboratoire de Chimie, CNRS, 351 cours de la Libératron, 33405 Talence Cedex, France

Received April 24, 1992; in revised form November 18, 1992; accepted November 24, 1992

Electrochemical oxidation in alkaline solution has been used to control and to extend the oxygen overstoichiometry of $La_2NiO_{4+\delta}$ phases ($0 \leq \delta \leq 0.25$). Chemical analysis has been carried out to determine the nickel (III) content and the related oxygen excess. Structural data (X-ray powder diffraction on $La_2NiO_{4+\delta}$ and neutron powder diffraction on $La_2NiO_{4.25}$) show that the interstitial oxygen atoms are introduced into the La_2O_2 layers. ESR spectra for the $La_2NiO_{4.25}$ compound recorded at 4.2 and 298 K characterize either low spin $Ni^{3+}(t_{2g}^6 d_{x^2-y^2}^1)$ in a flattened octahedral site or $Ni^{+}(t_{2g}^6 d_{z^2}^2 d_{x^2-y^2}^1)$ in an elongated octahedron. The results show that the relaxation of the structure as a function of δ could arise either from a steric effect (i.e., formation of Ni^{3+}) or from a disproportionation of Ni^{2+} into Ni^{+} and Ni^{3+}.

Introduction

The discovery of high temperature superconductivity in $La_2CuO_{4+\delta}$ phases has given rise to a large effort to understand the structural and physical properties of oxides of K_2NiF_4-type structure.

It is now well known, for instance, that $La_2NiO_{4+\delta}$ exists over a broad range of oxygen nonstoichiometry and that its structural, electric, and magnetic properties are very sensitive to the amount of oxygen present (*1–5*).

Dabrowski *et al.* (*4*) were the first authors to propose a phase diagram for $La_2NiO_{4+\delta}$ ($0 \leq \delta \leq 0.18$). They reported that for $0.03 \leq \delta \leq 0.13$ the system actually separates into two phases with the *Bmab* ($\delta \leq 0.03$) and the *Fmmm* ($\delta \geq 0.13$) space groups, respectively.

The $La_2NiO_{4+\delta}$ structure consists of *p*-type doped NiO_2 layers alternating with rock salt-type $La_2O_{2+\delta}$ layers of variable oxygen content, the sequence along the *c*-axis being NiO_2–$La_2O_{2+\delta}$. According to Jorgensen *et al.* (*5*), the excess oxygen atoms in the $\delta \geq 0.13$ samples are located within the La_2O_2 layers in a ($\frac{1}{4}$, $\frac{1}{4}$, 0.23) site (the (16*j*) Wyckoff position of the *Fmmm* structure). The additional oxygen atoms are bonded to four neighboring lanthanum atoms, which shifts the four nearest oxygen atoms from their normal position.

The nature and exact location of the extra oxygen atoms have raised many controversies; formation of superoxide (O_2^-) or peroxide (O_2^{2-}) anions has been proposed (*6, 7*).

Using the same electrochemical process as in the preparation of the $SrFeO_3$ cubic perovskite (*8*) or the $La_2CuO_{4+\delta}$ superconductor (*9*), $La_2NiO_{4+\delta}$ phases have been obtained at room temperature. The oxygen nonstoichiometry range has been extended up to $\delta = 0.25$. The structural properties of the system are discussed here as a function of δ in the light of a recent electron microscopy study (*10*) and of preliminary Rietveld structure refinements for $La_2NiO_{4.25}$ using neutron powder diffraction data. The oxidation states and electronic configurations of nickel cations are discussed on the basis of ESR measurements.

0022-4596/93 $5.00

Experimental

$La_2NiO_{4+\delta}$ ($\delta \leq 0.14$) samples were prepared from appropriate stoichiometric mixtures of NiO and La_2O_3 (treated at 800°C) dissolved in nitric aqueous solution. The solution of lanthanum and nickel nitrates was dehydrated at 200°C and slowly heated up to 700°C. Homogeneous samples with $La_2NiO_{4.14}$ composition were obtained after annealing for 48 hr at 1200°C in air and then quenching to room temperature. Samples with $La_2NiO_{4.03}$ compositions were also prepared by reducing $La_2NiO_{4.14}$ under flowing argon at 1300°C for 24 hr, followed by quenching under argon ($P_{O_2} \approx 10^{-2}$ atm). Pelletized samples (8 mm diameter, 2 mm thickness, 0.400 g) were finally sintered in the same conditions for 12 hr and then quenched. The density of the ceramics was close to 85% of the theoretical density for $La_2NiO_{4.14}$ and to 95% for $La_2NiO_{4.03}$.

The electrochemical oxidation procedure has previously been described in detail (*8*, *9*). A three-electrode device was used. The working electrode was a rotating polished disc (Rotating Disc Electrode) of $La_2NiO_{4.03}$ or $La_2NiO_{4.14}$ ceramic. The reference electrode was a HgO/Hg electrode (E_0 = +0.098 V/SHE). All potentials quoted in the present work are referred to this electrode. The auxiliary electrode was platinum foil. Experiments were carried out at 25°C in 1 *N* KOH solution under air. After the electrochemical process the ceramics were ground, then vigorously washed in distilled water under ultrasonics in order to remove any electrolyte pollution (K^+, OH^-, . . .), and finally immersed in ethanol before drying.

The samples before and after anodic polarization were characterized by XRD with a diffractometer using Cu$K\alpha$ radiation. The lanthanum concentration in the samples was determined using an F^- ion-selective electrode. The sample was dissolved in a 1 *N* HNO_3 solution and the lanthanum content was obtained by titration with a NaF solution according to the reaction $La^{3+} + 3F^- \rightarrow LaF_3$. The variation of the EMF of a cell containing a fluoride electrode (a LaF_3 single crystal), the solution to be analyzed, and a suitable reference electrode (a saturated calomel electrode) is in accord with the fluoride ion activity according to the Nernst equation at 25°C: $E = E' - 0.059 \log a_{F^-}$. In order to maintain a steady value of E', a buffer solution (TISAB solution) is added. The titration must be carried out in the 4–8 pH range: F^- ion species are stable only for pH > 4 and for pH > 8 the formation of $La(OH_3)$ takes place. This original method provides reliable and accurate results. The nickel content was determined using atomic absorption. These analyses led to a La/Ni ratio very close to 2. The concentration of holes, assuming they can be either on nickel cations or on oxygen atoms, was obtained by chemical analyses (iodometric titration and Mohr-salt analysis). The oxygen content was measured by TGA, which was carried out under a flow of N_2, 10% H_2 at a heating rate of 150°C/h. The complete reduction of the sample leads to La_2O_3 + Ni (see Fig. 1)). The experimental results are reported in Table I. One should note that the nickel (III) concentration is usually underestimated, as such highly oxidized cations may be reduced by water. All experimental composition values show good agreement.

Stoichiometric La_2NiO_4 was obtained by reducing $La_2NiO_{4.03}$ at 500°C under N_2, 10% H_2 flow, the oxygen stoichiometry being followed by TGA measurements (see Fig. 1).

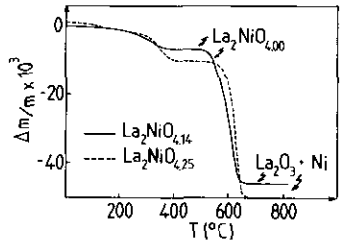

FIG. 1. TGA measurements on $La_2NiO_{4+\delta}$ compounds (δ = 0.14 and δ = 0.25) (heating rate 150°C/hr).

TABLE I

CHEMICAL ANALYSES OF $La_2NiO_{4+\delta}$ PHASES (IODOMETRIC TITRATION, MOHR-SALT ANALYSIS, TGA MEASUREMENTS) PREPARED BY SOLID STATE REACTION (*) AND BY ELECTROCHEMICAL OXIDATION (†)

Iodometric titration	Mohr-salt analysis	TGA	Composition
$La_2Ni^{2+}_{0.74}Ni^{3+}_{0.26}O_{4.13}$	$La_2Ni^{2+}_{0.70}Ni^{3+}_{0.30}O_{4.15}$	$La_2NiO_{4.15}$	$La_2NiO^{*}_{4.14}$
$La_2Ni^{2+}_{0.94}Ni^{3+}_{0.06}O_{4.03}$	$La_2Ni^{2+}_{0.90}Ni^{3+}_{0.10}O_{4.05}$	$La_2NiO_{4.03}$	$La_2NiO^{*}_{4.03}$
$La_2Ni^{2+}_{0.80}Ni^{3+}_{0.20}O_{4.10}$	$La_2Ni^{2+}_{0.76}Ni^{3+}_{0.24}O_{4.12}$	—	$La_2NiO^{\dagger}_{4.11}$
$La_2Ni^{2+}_{0.74}Ni^{3+}_{0.26}O_{4.13}$	$La_2Ni^{2+}_{0.72}Ni^{3+}_{0.28}O_{4.14}$	$La_2NiO_{4.16}$	$La_2NiO^{\dagger}_{4.14}$
$La_2Ni^{2+}_{0.70}Ni^{3+}_{0.30}O_{4.15}$	$La_2Ni^{2+}_{0.64}Ni^{3+}_{0.36}O_{4.18}$	—	$La_2NiO^{\dagger}_{4.17}$
$La_2Ni^{2+}_{0.66}Ni^{3+}_{0.34}O_{4.17}$	$La_2Ni^{2+}_{0.61}Ni^{3+}_{0.39}O_{4.19}$	—	$La_2NiO^{\dagger}_{4.18}$
$La_2Ni^{2+}_{0.57}Ni^{3+}_{0.43}O_{4.22}$	$La_2Ni^{2+}_{0.52}Ni^{3+}_{0.48}O_{4.24}$	—	$La_2NiO^{\dagger}_{4.23}$
$La_2Ni^{2+}_{0.56}Ni^{3+}_{0.44}O_{4.22}$	$La_2Ni^{2+}_{0.49}Ni^{3+}_{0.51}O_{4.26}$	$La_2NiO_{4.27}$	$La_2NiO^{\dagger}_{4.25}$

Results

Cyclic voltammograms (I, E) ($0 \leq E \leq 1$ V, sweep rate = 150 mV/min) are reported in Figs. 2a and 2b for $La_2NiO_{4.14}$.

The existence of a positive current intensity for low potentials (Fig. 2a, $100 \leq E \leq 500$ mV, C) can be related to the formation of the double layer capacitance depending on the electroactive surface (texture, morphology, etc.). As previously described (*11*, *12*), anodic potentials ($0 \leq E \leq 900$ mV) give rise to a surface oxidation of the sample (plateau O_I prior to an oxygen evolution (O_{II}) $4OH^- \rightarrow O_2 + 2H_2O + 4e^-$) according to the reaction $La_2NiO_{4.14} + \zeta OH^- \rightarrow La_2NiO_{4.14+\zeta/2} + \zeta/2\, H_2O + \zeta e^-$. This reaction leads to an increase of the trivalent nickel content on the surface. At decreasing potential, the reduction of oxygen and of trivalent nickel occurs in the wave R.

On the other hand, the change in the cyclic voltammograms (Fig. 2b) (second sweep after anodic polarization at 600 mV for 16 hours) confirms the increase of the trivalent nickel content on the surface. Such a surface oxidation ($M^{n+} \rightarrow M^{n+1} + e^-$) had indeed already been observed for perovskite-type oxides (*11*, *12*).

Experiments were carried out at 600 mV (plateau O_I just before the oxygen evolution) as a function of time (t). The variation of the OCV (open circuit voltage) potential vs polarization time for both $La_2NiO_{4.03}$ and

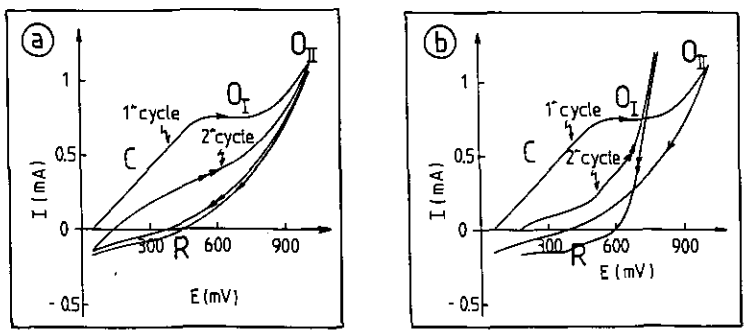

FIG. 2. Cyclic voltammograms (I, E) ($0 \leq E \leq 1$ V, sweep rate = 150 mV/min) for $La_2NiO_{4.14}$. (a) The successive voltammograms illustrate the formation of the double layer capacitance (C). (b) The second sweep has been obtained after anodic polarization at 600 mV for 16 hr.

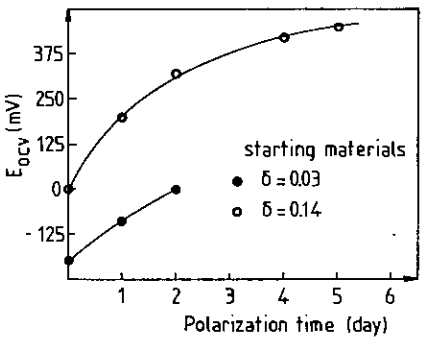

FIG. 3. Variation of the OCV potential as a function of polarization time for both $La_2NiO_{4.03}$ and $La_2NiO_{4.14}$ starting materials.

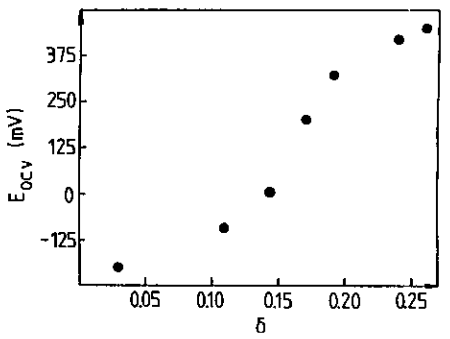

FIG. 5. Variation of the OCV potential vs excess oxygen amount δ for $La_2NiO_{4+\delta}$ compounds.

$La_2NiO_{4.14}$ is reported in Fig. 3. The value of this potential was determined after 30 min when steady-state conditions had been reached. The potential can be correlated to the Fermi energy level in the material, i.e., to the value of the Ni^{3+}/Ni^{2+} ratio. Its variation indeed indicates a drastic change, at least on the surface, of the material during the electrochemical treatment. In Fig. 4, the variation of the excess oxygen amount δ as a function of the polarization time shows that the maximum value of δ obtained under those conditions is close to 0.25, which is significantly higher than that obtained by the usual solid-state reactions (*5*). The OCV potential can be plotted vs δ (Fig. 5), which shows that its value can be used for the determination of the nickel (III) bulk concentration.

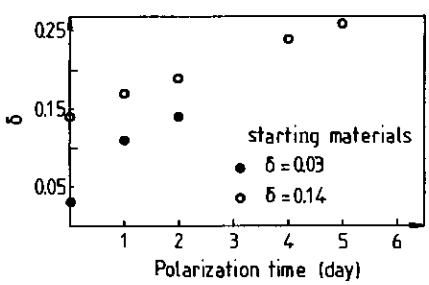

FIG. 4. Variation of the excess oxygen amount δ as a function of the polarization time for both $La_2NiO_{4.03}$ and $La_2NiO_{4.14}$ starting materials..

Structural data showing the variation of the cell parameters vs δ are reported in Figs. 6a and 6b and the diffractograms of $La_2NiO_{4+\delta}$ ($\delta = 0, 0.11, 0.14, 0.25$) are reproduced in Fig. 7. All these diffractograms give evidence that the electrochemically oxidized materials remain well crystallized. Therefore, neutron diffraction experiments of the most oxidized sample, $La_2NiO_{4.25}$, were carried out using the ILL high resolution diffractometer D2B in Grenoble, France. The sample was a pellet of 10 g (∅ 32 mm, thickness 2 mm), electrochemically oxidized and then ground into microparticles. The sample holder was made of vanadium and the wavelength employed was $\lambda = 1.594$ Å. The diffractograms ($13° \leq 2\theta \leq 155°$) were recorded at 298 K, and the data were collected for Rietveld structure refinement. In a recent study (*10*) electron microscopy observations of the $0.17 \leq \delta \leq 0.25$ phases have clearly shown the ordering of the extra oxygen atoms, leading to the formation of various commensurate or incommensurate superstructures. Triclinic unit cells have been proposed for the ordered line phases (corresponding to $\delta = \frac{1}{6}$ (≈ 0.17) and $\delta = \frac{1}{4}$ ($= 0.25$). This investigation has shown that the orthorhombic unit cell parameters determined by X-ray diffraction should be considered as average values because the symmetry involving oxygen ordering may vary and because of the existence of domains of close composition

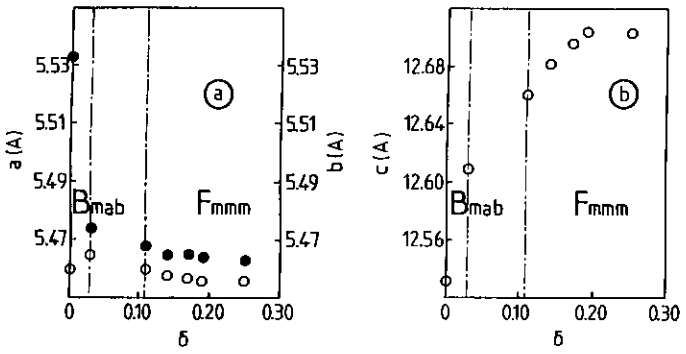

FIG. 6. Variation of the cell parameters vs excess oxygen amount δ in $La_2NiO_{4+\delta}$ phases: (a) a, $b = f(\delta)$; (b) $c = f(\delta)$.

within the material. Nevertheless, preliminary refinements for $La_2NiO_{4.25}$ were achieved with the *Fmmm* orthorhombic space group previously suggested by Jorgensen *et al.* (*5*) for the $La_2NiO_{4.18}$ phase. The oxygen interstitial defect O(4) (Fig. 8) was located at $(\frac{1}{4}, \frac{1}{4}, z \approx \frac{1}{4})$, while the apical oxygen atoms were split into two different positions, one remaining at the normal position O(2) (0, 0, z) and the other at a shifted site O(3) (x, y, z) due to the presence of the interstitial oxygen atoms O(4). Initial refinements (Table II), including 122 *Fmmm* Bragg reflections, were achieved with variable atom positions and variable site occupancies for O(4), O(3), and O(2). Only the temperature factors of O(2), O(3), and O(4) oxygen atoms were constrained. In these conditions, $B(O(2) = B(O(3)) = B(O(4)) = 0.70(8)$ Å^2 and the refined oxygen occupancy factors are respectively 1.12(3), 0.95(2), 0.22(1). The results of the refinement without constraints on the occupancy factor led

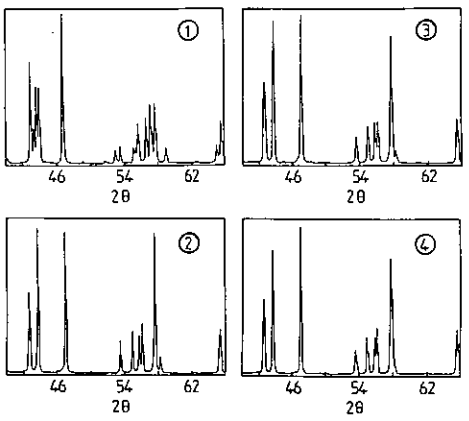

FIG. 7. Portion of X-ray diffractograms ($40° \leq 2\theta \leq 66°$): (1) $La_2NiO_{4.00}$ obtained by solid-state reaction; (2) $La_2NiO_{4.11}$ obtained by electrochemical oxidation; (3) $La_2NiO_{4.14}$ obtained by electrochemical oxidation; (4) $La_2NiO_{4.25}$ obtained by electrochemical oxidation.

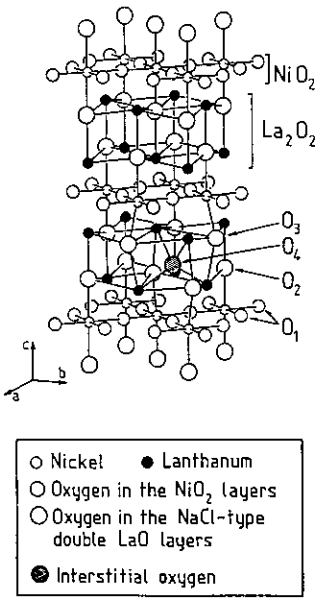

FIG. 8. Idealized structure of $La_2NiO_{4+\delta}$ ($\delta > 0.11$, *Fmmm* space group) according to Jorgensen *et al.* (*5*).

TABLE II

INITIAL REFINED STRUCTURAL PARAMETERS FOR $La_2NiO_{4.25}$

Space group			*Fmmm*		
Reliability factors (%)					
R_p			4.50		
R_{wp}			5.76		
R_I			6.20		
Unit cell parameters (Å)			a = 5.4644(1) b = 5.4570(1) c = 12.7035(2) V = 378.80(2) Å^3		
Atomic positions	X	Y	Z	B(Å)^2	n
La	0	0	0.3606(1)	0.60(2)	2
Ni	0	0	0	0.59(2)	1
O(1)	0.25	0.25	0	0.86(3)	2
O(2)	0	0	0.1762(4)	0.70(8)	1.12(3)
O(3)	−0.078(2)	−0.055(2)	0.1680(6)	0.70(8)	0.95(2)
O(4)	0.25	0.25	0.25(2)	0.70(8)	0.22(1)
Constraints			B(O(2)) = B(O(3)) = B(O(4))		

Note. The numbers in parentheses are standard deviations in units of the last significant digit. Where no standard deviation is given, the value has not been refined.

to excellent agreement with the $La_2NiO_{4.25}$ composition determined by chemical analyses, which validates the location of the interstitial oxygen atoms. One should note, on the basis of these refinements, that one O(4) interstitial oxygen atom affects four nearest neighbor O(3) atoms.

The final refinement was achieved with the following constraints:

$$n(\mathrm{O}(3)) = 4n(\mathrm{O}(4))$$

$$n(\mathrm{O}(2)) + n(\mathrm{O}(3)) = 2$$

$$B(\mathrm{O}(2)) = B(\mathrm{O}(3))$$

B(O(4)) not constrained.

The results of the final refinement are specified in Table III, and a portion of the Rietveld refinement profile is plotted in Fig. 9. The R values determined from powder diffraction data are relatively low and quite similar to those previously obtained for $La_2NiO_{4.18}$ by Jorgensen *et al.* (*5*). Some additional small peaks (arrows in Fig. 9) have not been taken into account in this refinement; refinements in the *Bamb* space group did not improve the R_I value. On the other hand, these peaks cannot correspond to magnetic reflections because the oxidized samples do not order, at least for temperatures higher than 1.5 K; the oxygen excess supresses 3D magnetic ordering (*13*). The presence of the small peaks probably arises from the ordering of the extra oxygen atoms, as suggested by the above-mentioned electron diffraction investigations, which implies that the real cell likely differs in symmetry from the orthorhombic *Fmmm* unit cell. Further calculations are now in progress.

ESR spectra of $La_2NiO_{4+\delta}$ samples were recorded using a Brucker 200H X-band spectrometer and the magnetic field was measured with a proton NMR probe. For the $\delta < 0.25$ sample no ESR signal was observed. On the other hand, for the $La_2NiO_{4.25}$ composition, a broad signal (ΔH = 550 G) was detected at room temper-

TABLE III

FINAL REFINED STRUCTURAL PARAMETERS FOR $La_2NiO_{4.25}$

Space group			*Fmmm*		
Reliability factors					
R_p			4.51		
R_{wp}			5.78		
R_I			6.27		
Unit cell parameters (Å)			a = 5.4644(1)		
			b = 5.4570(1)		
			c = 12.7035(2)		
			V = 378.80(2) Å^3		
Atomic positions	*X*	*Y*	*Z*	B(Å)^2	*n*
La	0	0	0.3606(1)	0.60(2)	2
Ni	0	0	0	0.60(3)	1
O(1)	0.25	0.25	0	0.86(3)	2
O(2)	0	0	0.1765(4)	0.47(6)	1.03(1)
O(3)	−0.073(2)	−0.053(2)	0.1683(6)	0.47(6)	0.97(1)
O(4)	0.25	0.25	0.246(8)	1.7(4)	0.24(1)
Constraints			n(O(3)) = 4n(O(4))		
			n(O(3)) + n(O(2)) = 2		
			B(O(2)) = B(O(3))		

Note. Numbers in parentheses are standard deviations in units of the last significant digit. Where no standard deviation is given, the value has not been refined.

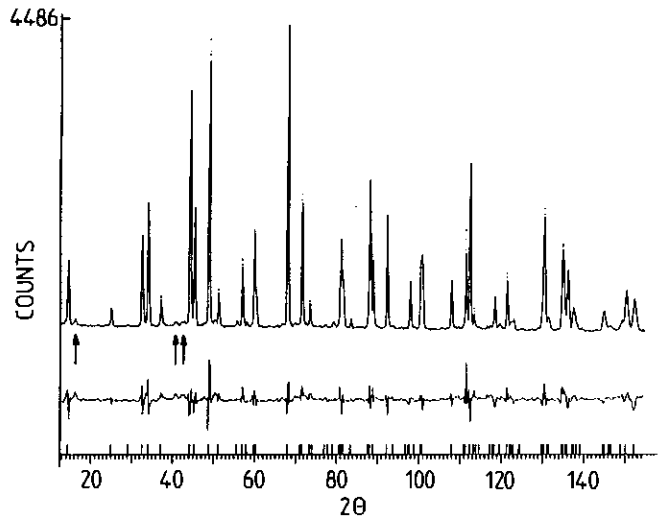

FIG. 9. Portion of the Rietveld refinement profile for orthorhombic (*Fmmm*) $La_2NiO_{4.25}$ at 300 K. Arrows show the peaks that have not been taken into account in the *Fmmm* space group.

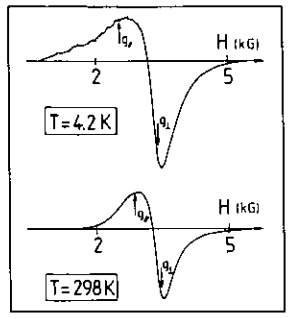

FIG. 10. ESR spectra for $La_2NiO_{4.25}$; the values of $g_\perp$ and $g_\parallel$ are indicated ($g_\perp = 2.03$; $g_\parallel = 2.33$).

ature, as well as at 4.2 K (Fig. 10). This signal can be assigned to a transition metal ion and not to O^- or O_2^- species, whose signal would be narrower and characteristic of an isotropic electronic distribution (the experimental O^- g-values are $g_\perp = 2.002$ and $g_\parallel = 2.07$ in hydroxide glasses, and $g_\perp = 2.001$ and $g_\parallel = 2.05$ in fluorosphosphates (*14*)). The ESR spectra of $La_2NiO_{4.25}$ indeed show an anisotropic electronic distribution. The values of $g_\parallel$ and $g_\perp$ factors were determined from simulated X-band spectra as $g_\parallel = 2.33 \pm 0.05$; $g_\perp = 2.03 \pm 0.02$; $\Delta H = 550$ G at 298 K leading to $\bar{g} = (g_\parallel + 2g_\perp)/3 = 2.13$.

Discussion

Although the *Fmmm* orthorhombic structure determined by X-ray diffraction for $\delta \geq 0.11$, which was used for the neutron diffraction refinements, is an average structure, it is worthwhile to discuss the structural data and their changes as a function of δ.

In agreement with Jorgensen *et al.* (*5*) the insertion of oxygen into the La_2NiO_4 network seems to lead to the formation of two orthorhombic phases with the *Bmab* ($0 \leq \delta \leq 0.03$) and the *Fmmm* ($\delta \geq 0.13$) space group, respectively. Intermediate compositions corresponding to $0.03 \leq \delta \leq 0.11$ in the two-phase domain have not been obtained by electrochemical oxidation; attention was essentially focussed on the phases with $La_2NiO_{4+\delta}$ ($\delta \geq 0.11$) compositions.

The variation of the orthorhombic distortion vs δ is quite different for both phases. For the *Bmab* phase the a-parameter strongly decreases with δ, while b remains almost constant. Both parameters tend to a common limit, nevertheless not reached, which would correspond to a straightening of the structure that would lead to the tetragonal *I4/mmm* symmetry. On the other hand, the *Fmmm* phase shows only a slight departure from tetragonal symmetry.

The orthorhombic structural distortion in the K_2NiF_4-type oxides has been widely discussed (*1*, *15*, *16*). One should point out that the stability of this structure made up of perovskite-type layers is governed by the value of the so-called Goldschmidt tolerance factor $t = (r_A + r_M)/\sqrt{2}\,(r_M + r_O)$, where r_A, r_M, and r_O are the ionic radii of A^{n+}, M^{m+}, and O^{2-} ions for a given A_2MO_4 compound. In the ideal condition ($t = 1$) the eight (A–O) distances are equal, which implies that the z coordinates of A and of the apical oxygen O(2) atoms are identical (Fig. 7). However, in most A_2MO_4 compounds, as well as in the AMO_3 perovskites, the size of the A-cation is often too small, which markedly lowers the t-value below 1. In the La_2MO_4 phases, as far as the $LaMO_3$ perovskite-type layers are concerned, this factor still indicates the departure from the ideal structure (tetragonal *I4/mmm* → orthorhombic *Bmab*). A significant decrease implies structural changes.

For instance in La_2NiO_4 and La_2CuO_4 for which t is equal to 0.885 and 0.868 respectively, the average distances are

$$\text{La–O(1)(Ni)} = 2.59 \text{ Å} \qquad \text{La–O(1)(Cu)} = 2.625 \text{ Å}$$

$$\text{La–O(2)(Ni)} = 2.805 \text{ Å} \qquad \text{La–O(2)(Cu)} = 2.76 \text{ Å}.$$

Thus, instead of forming eight long and weak bonds with respect to its size in the $LaMO_3$ perovskite-type layers, the lanthanum cation prefers to form four strong and four weak ones.

In addition, a ninth very strong bond with

the O(2) oxygen of the upper perovskite-type layer is formed, which provides the cohesion of the structure. This very short bond (2.33 Å $\ll r_{La^{3+}} + r_{O^{2-}} = 2.62$ Å) indicates the acidic character of La^{3+} and its tendency to form a complex LaO^+ ion. This linkage between the successive layers does not give rise to a particular stress in the structure. Conversely, within the (La_2O_2) layers, the very long La–O(2) distances create an equatorial compressive stress within the MO_2 sheet. This destabilizing stress strongly influences numerous structural, chemical, and electronic properties.

As previously quoted (*15*, *16*), from a structural point of view, the stress in the (*a*, *b*) plane leads to an alternating tilting of the MO_6 octahedra along the $[010]_{Bmab}$ direction; in other words, to buckling of the octahedra, yielding lattice parameters $b < a$ and a progression of the *I4/mmm* structure toward *Bmab* symmetry.

From the chemical viewpoint, this stress gives rise to an easy oxidation of M^{2+} to M^{3+} ions ($r_{M^{3+}} < r_{M^{2+}}$), so that the equatorial compressive stress gradually decreases. This is why the insertion of O(4) additional oxygen atoms in the La_2O_2 layers can be achieved relatively easily. It should also be emphasized that both oxidation of M^{2+} and introduction of additional oxygen relax the lattice (the lanthanum coordination increases and as a consequence the La–O average distances are enhanced). The overall process may be described in a formal manner by

$$M^{2+} + \frac{1}{n}\,O(4) \rightarrow M^{3+} + \frac{1}{n}\,O^{n-}(4).$$

Concerning the electronic properties, one can imagine that the equatorial compressive stress on the MO_6 octahedra may eventually favor an electron transfer of $\sigma^*_{x^2-y^2}$ antibonding electrons into the $\sigma^*_{z^2}$ states. As a consequence one can predict an elongation of the octahedra along the (001) axis even for a non-Jahn–Teller M^{2+} cation such as Ni^{2+}. For Ni^{2+} in *Oh* symmetry (with a ^3E_g ground term, $t_{2g}^6\sigma_{x^2-y^2}^1\sigma_{z^2}^1$) such a transfer would lead to a low spin state ($S = 0$) with the $t_{2g}^6\sigma_{z^2}^2\sigma_{x^2-y^2}^0$ configuration ($^1A_{1g}$ term in D_{4h} symmetry). Therefore, we may also expect that the compressive stress can be relieved due not only to structural distortion ($a \neq b$) but also because of a spin equilibrium ($S = 1$) $\Leftrightarrow$ ($S = 0$) that could be coupled with lattice phonons. In the same manner some disproportionation of divalent nickel may occur according to $2Ni^{2+} \Leftrightarrow Ni^+ + Ni^{3+}$ (i.e., $t_{2g}^6\sigma_{x^2-y^2}^1\sigma_{z^2}^1 \Leftrightarrow t_{2g}^6\sigma_{x^2-y^2}^1\sigma_{z^2}^2 + t_{2g}^6\sigma_{x^2-y^2}^0\sigma_{z^2}^1$), which could induce such a structural stabilization. Both intra and interatomic transfers probably occur simultaneously.

The variation of the *a*- and *b*-parameters in the *Bmab* phase indicates a straightening of the MO_6 octahedra as expected from a steric point of view, but this cannot result merely from the slight oxidation of the material ($\delta \leq 0.03$; no more than 6% of Ni^{2+} is transformed into Ni^{3+}). Therefore, one can presume that a dynamic spin equilibrium, possibly even a static one at very low temperature, would be responsible for the small distortion. For the pseudotetragonal *Fmmm* phase ($\delta \geq 0.11$) relief of the internal stresses results from both effects previously described, the insertion of oxygen into the (La_2O_2) layers (steric effect) and the oxidation of the (NiO_2) layers (electronic effect). The small decrease in *a*- and *b*-parameters agrees with the increasing oxidation state of nickel. For $\delta \leq 0.17$) the enhancement of *c* is essentially a consequence of the insertion of oxygen into the (La_2O_2) layers. On the other hand, the absence of changes in *c* for $\delta \geq 0.17$ could result from the fact that the previous steric effect is now more strongly compensated by electronic effects in the (NiO_2) layer.

The interatomic distances in $La_2NiO_{4.25}$ calculated from a Rietveld structure refinement are reported in Table IV. They indeed are characteristic of the relaxation of the structure. The La–O distances increase and the lanthanum polyedron appears more regular than in $La_2NiO_{4.00}$. In addition, the Ni–O(1) distance is shortened. Both effects

TABLE IV

INTERATOMIC DISTANCES (Å) IN $La_2NiO_{4.25}$ AND IN $La_2NiO_{4.00}$ FROM RIETVELD REFINEMENTS OF NEUTRON POWDER DIFFRACTION DATA

	$La_2NiO_{4.25}$ (this work)	$La_2NiO_{4.00}$ (according to Jorgensen *et al.*) (5)
LaO_9 polyhedra		
La–O(1)	2.624(1)(×4)	2.538(3)(×2)
		2.654(3)(×2)
La–O(2)	2.332(5)	2.324(4)
	2.771(3)(×2)	2.789(8)(×2)
	2.768(4)(×2)	2.569(4)(×2)
La–O(3)[a]	2.38(1)–2.50(2)	
La–O(4)[a]	2.36(1)–2.41(1)	
NiO_6 octahedra		
Ni–O(1)	1.9306(1)(×4)	1.9486(2)(×4)
Ni–O(2)	2.242(3)(×2)	2.261(4)(×2)
Ni–O(3)	2.19(1)(×2)	
O(1)–O(n) distance		
O(1)–O(1)	2.728(1)(×2)	2.7328(1)(×2)
	2.732(1)(×2)	2.7785(7)(×2)
O(1)–O(2)	2.958(2)(×4)	2.972(4)(×2)
		2.994(1)(×2)
O(1)–O(3)[a]	2.58(1)–2.97(2)	

Note. Numbers in parentheses are standard deviations in units of the last significant digit.

[a] Only the shortest and the longest distances have been reported.

tend to relieve the constraint. The O(2)–O(3) and O(3)–O(4) distances have not been reported, since in the *Fmmm* space group, the O(2), O(3), and O(4) sites are randomly occupied. In addition, as far as the (NiO_6) octahedra are concerned, the displacement of the O(2) oxygen atoms into the O(3) site (= 0.5 Å) involves the formation of two types of elongated (NiO_6) octahedra with $d^{\parallel}_{Ni-O} = 2.242$ Å and $d^{\parallel}_{Ni-O} = 2.194$ Å.

The ESR results obtained for $La_2NiO_{4.25}$ ($g_{\parallel} = 2.33 > g_{\perp} = 2.03$) can be interpreted in various ways: the unpaired electron is obviously located in the $d_{x^2-y^2}$ orbital, giving rise either to trivalent nickel ions with the $t_{2g}^6 d_{x^2-y^2}^1$ electronic configuration or possibly, to monovalent nickel ions with the $t_{2g}^6 d_{z^2}^2 d_{x^2-y^2}^1$ configuration. In the first case the trivalent nickel may be assumed to accommodate a flattened octahedral site. This configuration of trivalent nickel has actually been observed only seldom. However, as a result of the bond competition in $SrNdAl_{0.93}Ni_{0.02}O_4$, Ganguly (*17*) observed an ESR signal characterizing trivalent nickel in such a flattened octahedral site with $g_{\parallel} = 2.25$ and $g_{\perp} = 2.05$, which are close to our experimental values. In the second case, the monovalent nickel should occupy an elongated octahedron. A similar ESR signal has been observed in irradiated $Li_{1-x}Ni_xF$ (*18*) corresponding to Ni^+ in a stretched octahedral site ($g_{\parallel} = 2.53$ and $g_{\perp} = 2.10$).

The observed ESR signal could also be characteristic of trivalent nickel in an elongated octahedron ($t_{2g}^6 d_{z^2}^1$ configuration) but with antiferrodistortive ordering ($g_{\parallel c} = g_{\perp}$ and $g_{\perp c} = \frac{1}{2}(g_{\parallel} + g_{\perp})$). In this case the values of $g_{\perp c}$ and $g_{\parallel c}$ would be equal to 2.03 and 2.33, respectively. However, these values lead to unphysical calculated values of $g_{\parallel}$ ($g_{\parallel} < 2$) and does not seem to correspond to antiferrodistortive trivalent nickel ($t_{2g}^6 d_{z^2}^1$). On the other hand, no ESR signal has been detected for $\delta < 0.25$. The existence of intralayer antiferromagnetic interactions in $La_2NiO_{4+\delta}$ ($\delta < 0.25$) probably accounts for the disappearance of the ESR signal. Thus, two hypotheses (Ni^{3+}: $t_{2g}^6 d_{x^2-y^2}^1$ or Ni^+: $t_{2g}^6 d_{z^2}^2 d_{x^2-y^2}^1$) must be taken into consideration for $La_2NiO_{4.25}$. Magnetic susceptibility measurements as a function of temperature are in progress in order to decide between these assumptions.

The existence of Ni^{3+} cations in the $t_{2g}^6 d_{x^2-y^2}^1$ electronic configuration implies flattened octahedral sites. Rietveld structure refinement indeed shows a decreasing Ni–O(2) distance ($d_{Ni-O(3)} < d_{Ni-O(2)}$), which means that the O(4)–O(2) electrostatic repulsion (steric effect) would produce a stress on the Ni–O(2) bond. However, the octahedral site does not seem to be flattened but, as pointed out before, the data should be considered as average distances. Conversely, the formation of Ni^+ might result from a disproportionation of Ni^{2+} (schemat-

ically $2Ni^{2+} \Leftrightarrow Ni^{+} + Ni^{3+}$), as previously suggested for La_2NiO_4 (*15*), where the disproportionation would in fact represent a two-dimensional charge density wave involving the equilibrium

$$2Ni^{2+} \Leftrightarrow Ni^{(2+\delta)+} + Ni^{(2-\delta)+} \quad (16)$$

Further experiments are needed to ascertain the electronic configuration of the nickel cations.

Conclusion

The electrochemical oxidation in alkaline solution has been proved to be an efficient tool for extending the oxygen over-stoichiometry of $La_2NiO_{4+\delta}$. Values up to $\delta = 0.25$ have been reached. Structural data allow us to conclude that the introduction of interstitial oxygen atoms occurs in the (La_2O_2) layers, which involves in a first stage a relaxation of the structure resulting from steric effects. The structure becomes almost tetragonal ($I_{4/mmm}$, $a \approx b$) and the c parameter continuously increases with δ up to $\delta = 0.17$. Nickel(II) is oxidized into nickel(III) and the absence of ESR signal for $\delta < 0.25$ could be related to the presence of antiferromagnetic interactions in $La_2NiO_{4+\delta}$.

For highly oxidized samples, typically for $\delta \geq 0.17$, electronic features become dominant and the insertion of oxygen seems to be fully explained by electronic phenomena. On the basis of an ESR investigation of $La_2NiO_{4.25}$, two hypotheses have been taken into consideration:

—The presence of Ni^{3+} $(t_{2g}^6 d_{x^2-y^2}^1)$ in a flattened octahedral site due to the O(4)–O(2) electrostatic repulsion (steric effect).

—The presence of Ni^{+} $(t_{2g}^6 d_{z^2}^2 d_{x^2-y^2}^1)$ in an elongated octahedral site which would result from a disproportionation of Ni^{2+} (electronic effect).

Based on an electron microscopy study (*10*) a more thorough Rietveld structure refinement of the neutron diffraction data, taking into account the interstitial oxygen ordering, is in progress in order to determine the exact structure of $La_2NiO_{4.25}$ and to understand the transport properties of this material.

References

1. C. N. R. Rao, P. Ganguly, K. K. Singh, and R. A. Mohan Ram *J. Solid State Chem.* **72,** 14 (1988).
2. R. R. Schartman and J. M. Honig, *Mater. Res. Bull.* **24,** 1375 (1989).
3. T. Freltoft, D. J. Buttrey, G. Aeppli, D. Vakmin, and G. Shirane, *Phys. Rev. B* **44,** 5046 (1991).
4. B. Dabrowski, J. D. Jorgensen, D. G. Hinks, S. Pei, D. R. Richards, H. B. Vanfleet, and D. L. Decker, *Physica C* **162–164,** 99 (1989).
5. J. D. Jorgensen, B. Dabrowski, S. Pei, D. R. Richards, and D. G. Hinks, *Phys. Rev. B* **40,** 2187 (1989).
6. M. Strongin, S. L. Qiu, J. Chen, C. L. Lin, and E. M. McCarron, *Phys. Rev. B* **41,** 7328 (1990).
7. C. Chaillout, J. Chenevas, S. W. Cheong, Z. Fisk, M. Marezio, B. Morosin, and J. E. Shirber, *Physica C* **170,** 87 (1990).
8. A. Wattiaux, L. Fournes, A. Demourgues, N. Bernaben, J. C. Grenier, and M. Pouchard, *Solid State Commun.* **77,** 489 (1991).
9. J. C. Grenier, A. Wattiaux, N. Lagueyte, J. C. Park, E. Marquestaut, J. Etourneau, and M. Pouchard, *Physica C* **173–174,** 139 (1991).
10. A. Demourgues, F. Weill, J. C. Grenier, A. Wattiaux, and M. Pouchard, *Physica C* **192,** 425 (1992).
11. A. Wattiaux, J. C. Grenier, M. Pouchard, and P. Hagenmuller, *J. Electrochem. Soc.* **134,** 1714 (1987); *J. Electrochem. Soc.* **134,** 1718 (1987).
12. S. Trasatti, "Electrodes of Conductive Metallic Oxides," p. 261, Elsevier, Amsterdam.
13. J. Rodriguez-Carvajal, M. T. Fernandez-Diaz, and J. L. Martinez, *J. Phys. Condens. Matter* **3,** 3215 (1991).
14. J. H. Lunsford and J. P. Jayne, *J. Chem. Phys.* **44,** 1487 (1966).
15. K. K. Singh, P. Ganguly, and J. B. Goodenough, *J. Solid State Chem.* **53,** 254 (1984).
16. P. Ganguly and C. N. R. Rao, *J. Solid State Chem.* **53,** 193 (1984).
17. P. Ganguly, Ph.D. thesis, University of Bordeaux I (1984).
18. M. O. M. O'Brien, *Proc. Roy. Soc. Ser. A* **281,** 323 (1964).